Rotor Dynamics of Centrifugal Compressors in Rotating Stall

Authored by:

Donald E. Bently

Founder, Chairman, and CEO
Bently Nevada Corporation, and
President
Bently Rotor Dynamics Research Corporation
e-mail: don@bently.com

Paul Goldman

Manager
Bently Rotor Dynamics Research Corporation
e-mail: paul.goldman@bently.com

Jing Yuan

Senior Research Engineer
Bently Rotor Dynamics Research Corporation
e-mail: jing.yuan@bently.com

This paper discusses rotating stall in centrifugal compressors from the standpoint of rotor dynamics. The literature survey shows insufficient understanding of rotor dynamic implications of rotating stall. Most of the literature on the subject addresses only aerodynamic aspects of the problem, thus putting an emphasis on stall cells, with exclusion of the rotor vibrational response. This paper treats a compressor as a coupled mechanical-aerodynamic system. For the rotor/fluid system, the results of Dynamic Stiffness identification of an experimental centrifugal compressor in rotating stall and in normal operating conditions are presented. It is shown that the aerodynamically-induced radial (direct spring) stiffness coefficients are negative in normal operating conditions. The negative radial stiffness effect in the case of rotating stall is even more profound. The result is that the rotor system's mechanical resonance could be reduced to as low as 5% to 10% of running speed. The conclusion is that the rotor dynamic stability margin during rotating stall is reduced.

Introduction

The interest in radial compressor fluid-induced instabilities started in the mid-seventies. Since then, a number of case histories of high-pressure centrifugal compressor instabilities have been published [1-17]. Most of the publications report two types of rotor vibrational behavior: 1) high eccentricity and rotor first natural frequency re-excitation; 2) subsynchronous forward precession with rotative speed-dependent frequency. The former is usually referred to as whip-type behavior and is normally associated with balance pistons, fluid-film bearings, and labyrinth seals. The latter is called whirl-type behavior [27-28] and can be associated either with fluid-film bearings/seals or with rotating stall. Rotating stall usually results in an appearance of a low subsynchronous frequency component in the rotor vibration spectrum (frequency ratios fall typically between 8% and 40%, but can go as high as 80%, of rotative speed [20]). The emphasis on rotor behavior does not allow for details of particular flow patterns, but treats the fluid (gas) "in average," which falls in the scale of rotor motion.

Experimental Compressor for Rotating Stall

An experimental rig (Figure 1) is constructed to evaluate Dynamic Stiffness for the rotor/fluid system during rotating stall and during normal operating conditions. The rig consists of a single-stage centrifugal compressor with a vaneless diffuser, driven by a 1-hp dc electric motor. The motor speed is controlled by a high-output, variable power supply, and the speed can be controlled from near zero to 17,000 rpm. The motor is attached to the compressor rotor by a flexible disk coupling.

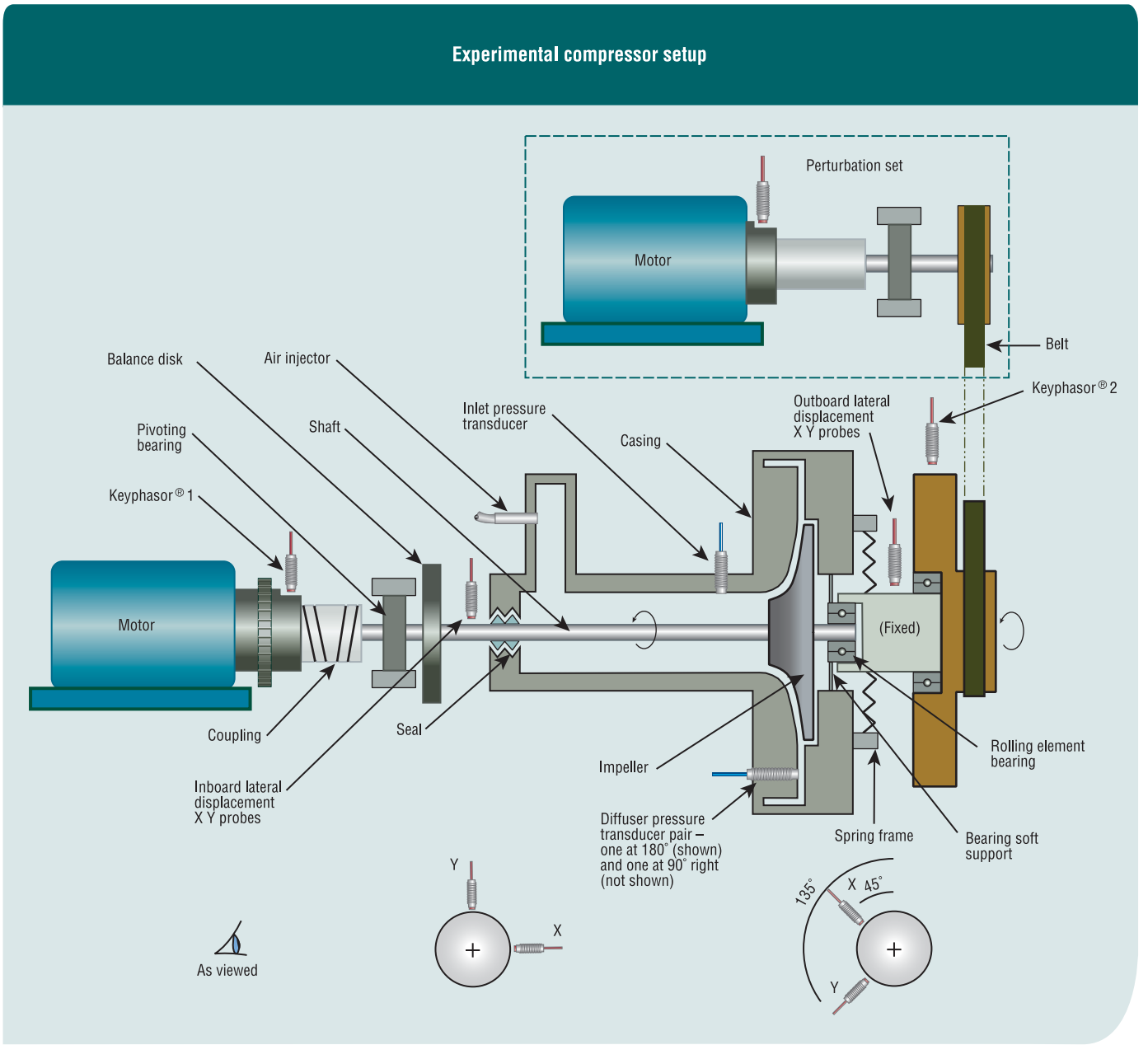

Figure 1.

The compressor rotor is separated into two pieces: 1) a rotating section from the motor to the outboard end of the compressor; and 2) a nonrotating stub shaft from the outboard compressor bearing to the outermost support bearing. The rotating section is supported by two bearings: 1) a pivoting bearing on the driver-end; and 2) a rolling-element bearing on the nondriver-end in a soft support. A spring-load frame is attached to the nondriver-end of the nonrotating stub shaft to control the radial position of the compressor rotor and counteract the gravity load of the rotor. The nonrotating stub shaft also provides the input for the perturbation set. The nonsynchronous perturbator transmits an exciting rotating force with variable frequency to the compressor rotor with a constant rotating force, 1.3 N.

Two orthogonal pairs of eddy current displacement transducers are mounted next to the inboard bearing and at the spring-load frame to measure the displacement of the rotor. Two Keyphasor® probes are installed on the compressor shaft and the perturbator disk to provide

Differential pressure (outlet minus inlet) versus airflow

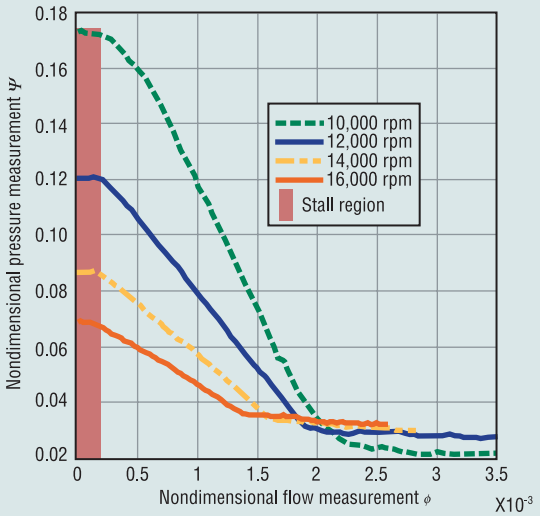

Figure 2.

Direct orbit plot of the outboard lateral vibration data in rotating stall operating conditions. 1-8 are consecutive Keyphasor® numbers.

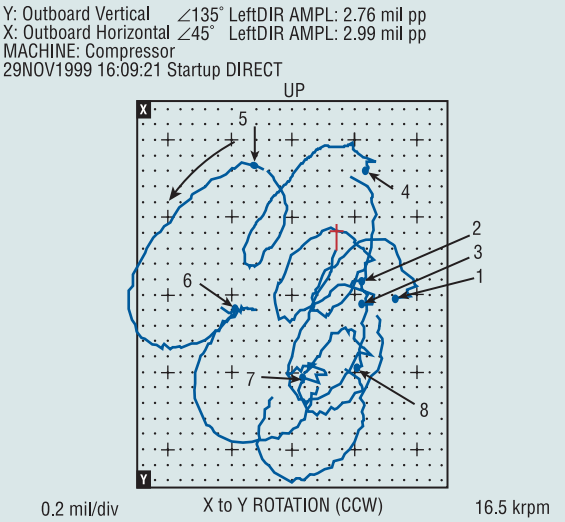

Figure 4.

Waterfall plot generated from the outboard lateral vibration data with increasing airflow.

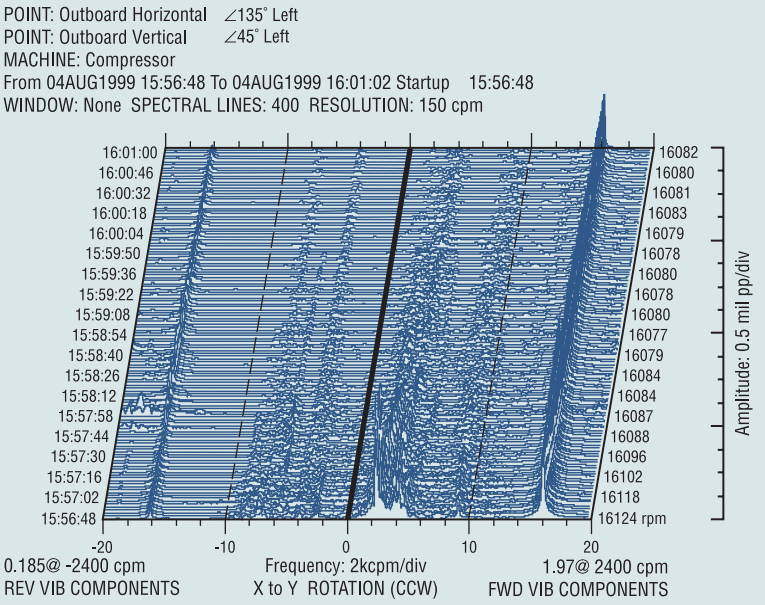

Figure 3.

phase and speed references. A conical exhaust valve on a lead screw controls airflow through the compressor. The valve is located at the end of the discharge pipe from the compressor (not shown in Figure 1). It can be adjusted by several turns from fully closed, which completely blocks the output flow of the compressor. When the valve is fully opened, the airflow passes with minimum restriction. The actual flow is monitored by a flowmeter. Dynamic pressure transducers measure the compressor inlet and discharge pressure, as well as pressure wave propagation in the diffuser (at the same radius, 90° apart).

Compressor Performance

An experimental compressor performance chart is displayed in Figure 2, nondimensionally, applying general conversion rules as in [27].

As observed in Figure 2, the pressure drops with the increase of

Full spectrum cascade plot of the outboard lateral vibration data in rotating stall operating conditions.

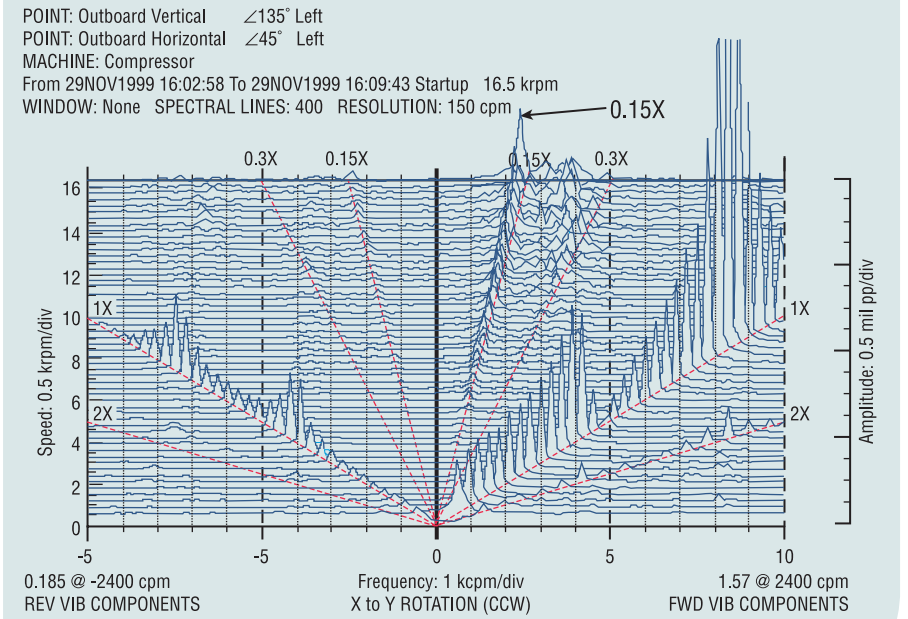

Figure 5.

airflow, and the compressor operates outside the rotating stall regime. Increasing the airflow stabilizes the compressor. The phenomena is supported by the full spectrum waterfall data, Figure 3, taken at a constant rotative speed with the flow increased by opening the exhaust valve from fully closed to wide open.

Rotating Stall Experiments of Compressor Startups

Under the flow constriction conditions, the experimental compressor rotor exhibits rotating stall whirl with a subsynchronous frequency component of 0.15X in the forward direction, presented in Figures 4 to 6. Compared to the field case history above, the orbits (Figure 4) show a clear forward precession with a frequency of 0.15X, supported by full spectrum cascade data (Figure 5) generated from the lateral vibration. In addition, full spectrum cascade data (Figure 6) is generated from the pressure transducers, mounted in the diffuser, further substantiating this result.

Nonsynchronous Perturbation Tests

A series of nonsynchronous perturbation tests were performed at each of four compressor running speeds: 10,000; 12,000; 14,000; and 16,000 rpm. For the detailed description of the applied Methodology, see [29]. At each running speed, perturbation

Full spectrum cascade plot generated from diffuser pressure transducers, positioned 90° apart, in rotating stall operating conditions.

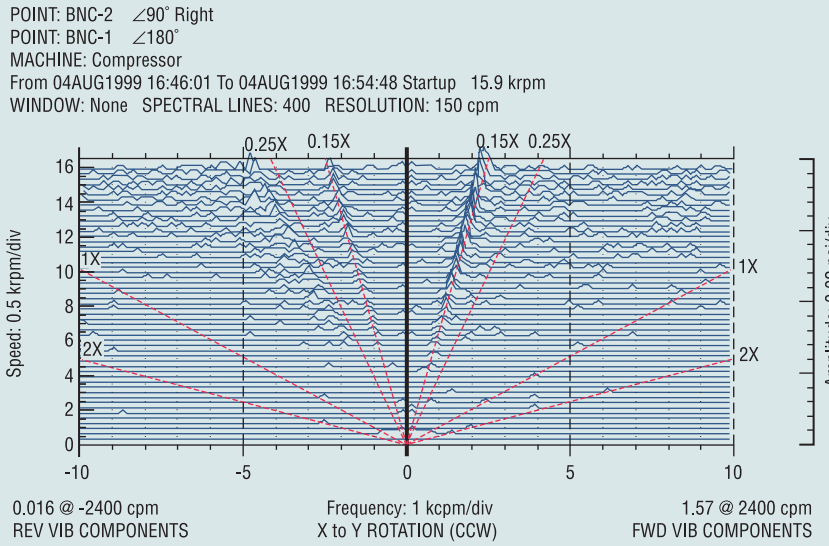

Figure 6.

runs were performed using two different valve positions: the first to put the compressor into rotating stall and the second to put the compressor in normal operating conditions. These two valve positions were placed as close together as possible to exhibit rotating stall. The perturbator generated a force of magnitude F with orientation δ rotating in the same direction as the compressor rotation (forward perturbation), resulting in the perturbation vector $Fe^{j\delta}$. The perturbator was revved up from slow-roll speed to 5,000 rpm, in order to identify Dynamic Stiffness of the rotor first mode. The vibration signals from two orthogonal eddy current displacement transducers (see Figure 1 for probe orientation) were filtered to the frequency ω of the perturbation force. This yielded amplitudes and phases for vertical (Y) and horizontal (X) components of the response.

In order to minimize the influence of mechanical stiffness asymmetry, 1X vertical $\left(\vec{Y}_\omega\right)$ and horizontal $\left(\vec{X}_\omega\right)$ vectors were combined into the circular forward (in the direction of perturbation) component:

$$\vec{A}_\omega^{(fwd)} = \vec{Y}_\omega + j\vec{X}_\omega \qquad [1]$$

Next, the perturbation process was repeated for the perturbation in a direction opposite the rotation of the compressor rotor (reverse perturbation) for each running speed, Ω, and valve setting. In this case, the forward (in the direction of perturbation) component of the filtered-to-perturbation-frequency response was opposite the direction of rotation. The nonsynchronous Dynamic Stiffness was calculated as in equation [2] by taking the ratio of the force input to the response vectors for each speed in the database.

$$DS(\omega) = DDS(\omega) + jQDS(\omega) = \frac{Fe^{j\delta}}{\vec{A}_\omega^{(fwd)}},$$
$$\text{where} \quad DDS(\omega) = direct\,(DS), \qquad [2]$$
$$QDS(\omega) = quadrature\,(DS)$$

Forward and reverse perturbation data generated in normal operating conditions. (a) Response phases and amplitudes of the rotor outboard lateral. (b) Direct and Quadrature Dynamic Stiffness.

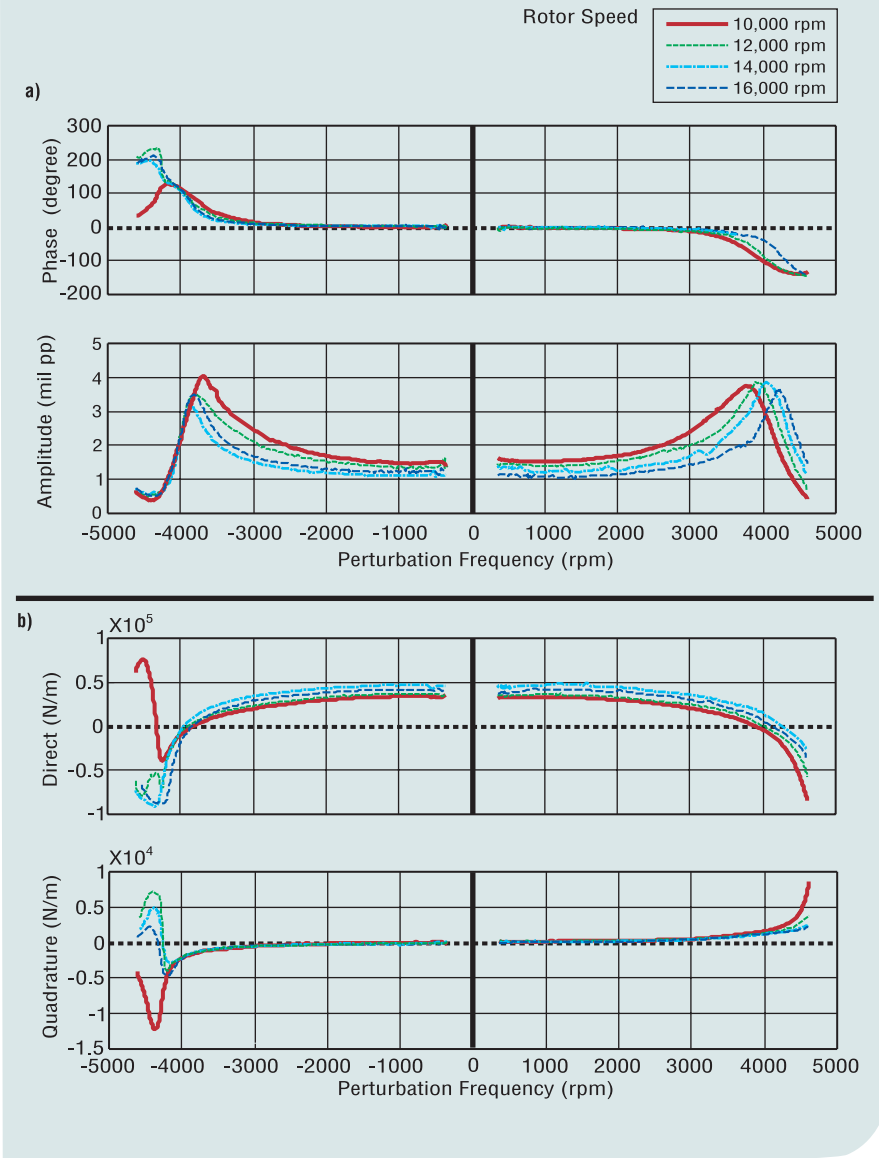

Figure 7.

Figures 7 and 8 present the forward and reverse perturbation data with the results of Dynamic Stiffness under the test conditions described above. The negative speed corresponds to reverse perturbation conditions.

Both figures show that in the forward direction, the Direct Dynamic Stiffness increases as the rotor speed increases, but in the reverse direction, the Direct Dynamic Stiffness stays about the same value for all rotor speeds. This phenomenon indicates the effect of the fluid inertia.

Since the total Dynamic Stiffness of the compressor consists of mechanical and aerodynamic parts, the former is measured by running nonsynchronous perturbation on the compressor at zero rotative speed (DS_0). The difference of Dynamic Stiffness between the running compressor and stopped compressor represents aerodynamically-induced Dynamic Stiffness, DS_{air}:

$$\begin{aligned} DSS_{air}(\omega) &= direct(DS - DS_0) \\ &= K_{air} - M_{air1}\omega^2 - M_{air2}(\omega - \lambda\Omega)^2 \\ QDS_{air}(\omega) &= quad(DS - DS_0) \\ &= D_{air}(\omega - \lambda\Omega) \end{aligned} \quad [3]$$

where M_{air1} , K_{air} , D_{air} are air inertia, radial stiffness, and damping respectively, generated by the air/impeller interaction. M_{air2} is a fluidic mass effect term, and λ represents a swirling ratio coefficient.

Equation [3] shows the parameters of Direct and Quadrature Dynamic Stiffness extrapolation. The results of the raw data and the described processed data are illustrated in Figures 9 and 10. Figure 9 shows the negative values for air-induced radial stiffness. The swirling ratio coefficient λ is shown in Figure 10. The negative value of λ indicates the reverse-flow pattern rotation. It becomes stronger at lower rotor rotative speeds and in the rotating stall operating conditions.

Equation [3] also allows performing eigenvalue calculations for the compressor rotor dynamic stability evaluation,

Forward and reverse perturbation data generated in rotating stall operating conditions. (a) Response phases and amplitudes of the rotor outboard lateral. (b) Direct and Quadrature Dynamic Stiffness.

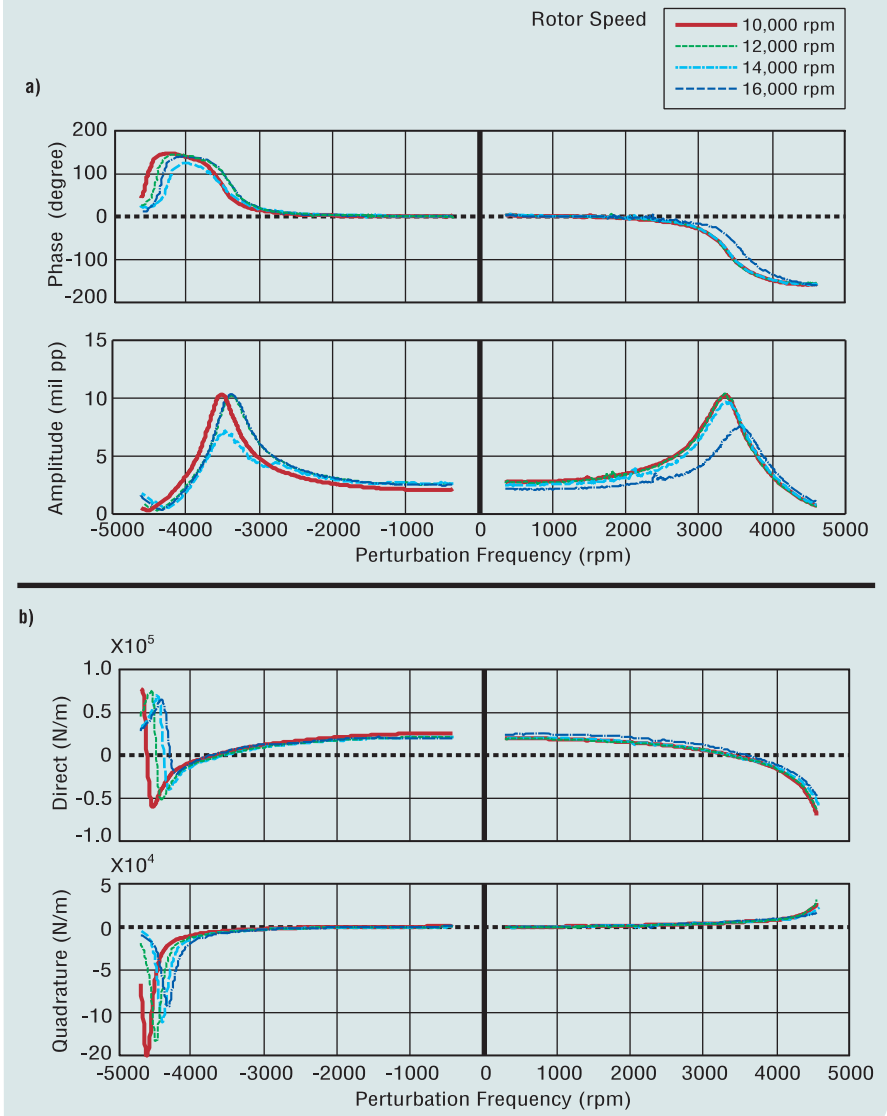

Figure 8.

Air-induced radial stiffness calculated in rotating stall and normal conditions with rotative speed changes.

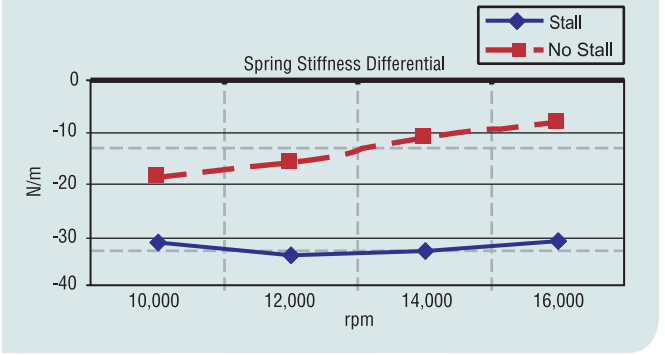

Figure 9.

Swirling ratio coefficient, λ, in rotating stall and normal conditions with rotative speed changes.

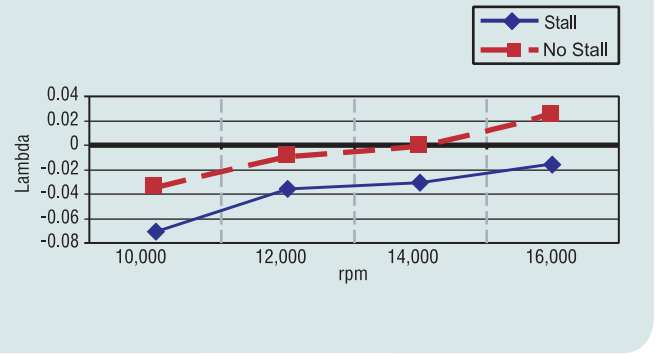

Figure 10.

shown in Figure 11. The eigenvalue analysis clearly shows that the rotating stall lowers radial stiffness and decay rates. In the case of rotating stall, increasing the rotative speed increases the rotor stability margin. The result of eigenvalue analysis shows that rotating stall not only lowers the rotor radial stiffness, but also brings the compressor toward the edge of the instability.

Another set of perturbation tests was performed for increased airflow of the compressor. The tests also included forward and reverse perturbations with two rotative speeds of the compressor rotor. In order to produce the Dynamic Stiffness (Figure 12b) from the perturbation data (Figure 12a), the same routine was used as in Equations [1] and [2]. The same concept of

Eigenvalues for rotor in rotating stall and normal conditions comparing to mechanical model.

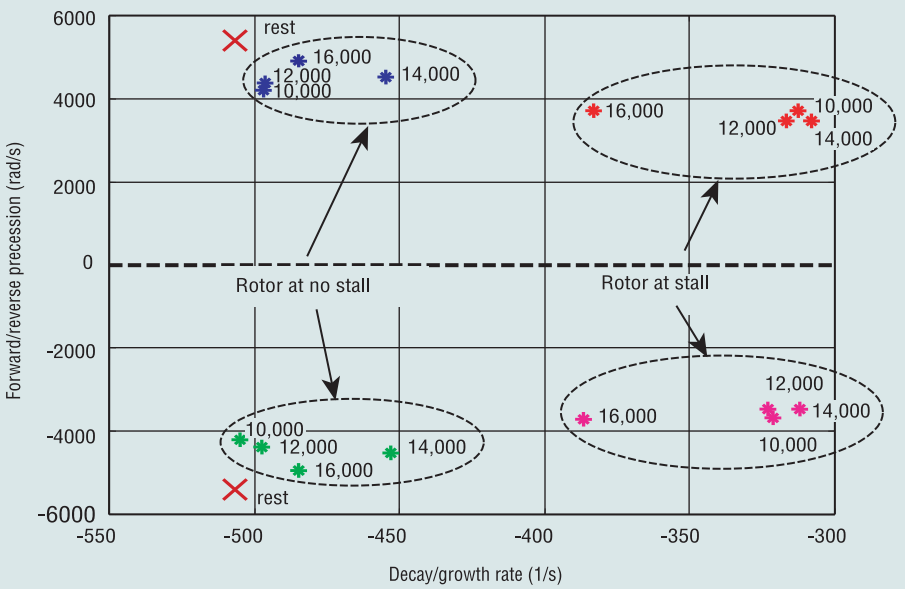

Figure 11.

subtracting the mechanical Dynamic Stiffness from the total Dynamic Stiffness (Equation [3]) was used to determine the aerodynamic part of Dynamic Stiffness. The results are illustrated in Figures 13 and 14. They show that the airflow increased the Direct Dynamic Stiffness (Figure 12b). This offset the negative effect of the radial stiffness induced aerodynamically (Figure 13).

The swirling ratio coefficient λ became positive as the airflow increased (Figure 14). Figure 15 shows the result of the corresponding eigenvalue calculations, showing that when the airflow became stronger, the compressor moved away from the rotating stall regime and became more stable.

Forward and reverse perturbation data generated in rotating stall conditions at rotative speed 16,000 rpm. (a) Lateral response phase and amplitude at the rotor outboard. (b) Direct and Quadrature Dynamic Stiffness.

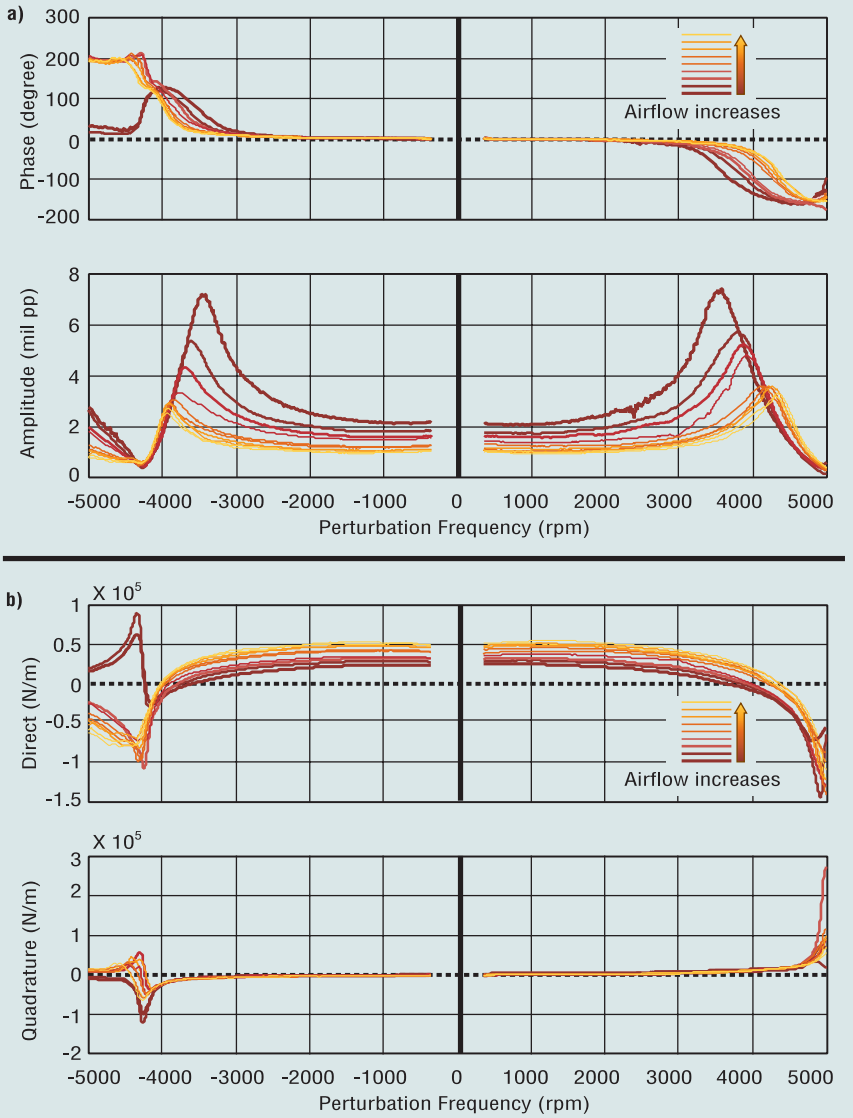

Figure 12.

Conclusions

This paper provides some insight into the rotor dynamic implications of the phenomenon of rotating stall. It fills the gap in the literature, which all but ignores the rotor dynamic implication of rotating stall. The most significant conclusion from this paper is that aerodynamic forces applied to the impeller generate negative radial stiffness (stiffness K_{air} appears negative in all experiments). It is also important that this stiffness drops even more during the rotating stall. In short, the conclusions can be made as follows:

The rotating stall conditions manifested themselves in the rotor lateral vibration signature as rotor forward precession with subsynchronous frequency, which tracks the rotor speed. This behavior is referred to as a rotating stall whirl.

The parameter clearly identified by nonsynchronous perturbation tests is aero-dynamically-induced radial stiffness. In all conditions, it is negative. From the practical standpoint, it means that even in normal operating conditions, centrifugal compressors have lower natural frequencies than appear in purely mechanical calculations.

The aerodynamically-induced radial stiffness during

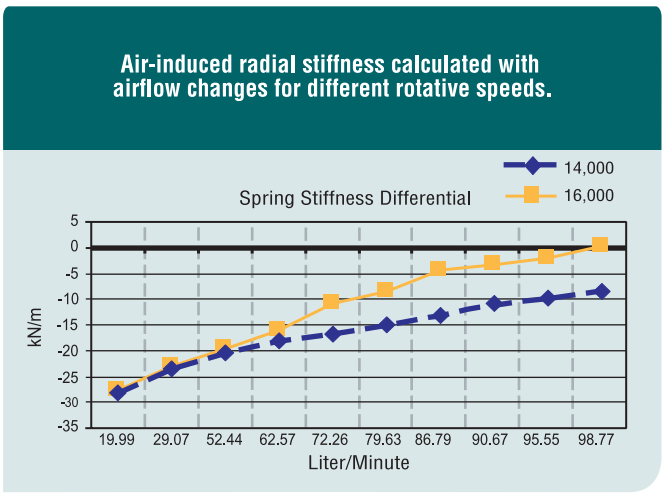

Figure 13.

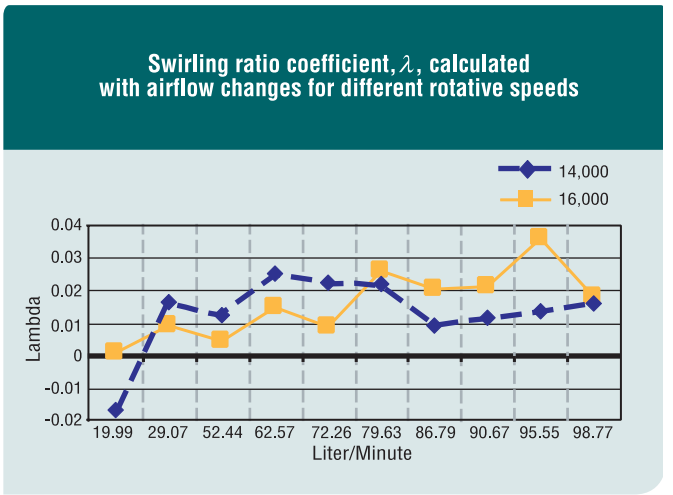

Figure 14.

rotating stall drops dramatically and ultimately can make a compressor unstable. The data from field case histories indicates that the resulting mechanical resonance can be driven by rotating stall to as low as 5% to 10% of running speed.

Altogether, aerodynamic forces may have a significant destabilizing effect on the compressor. In the case of a flexible rotor and/or soft bearings, these forces are able to create a rotor dynamic instability of whirl type.

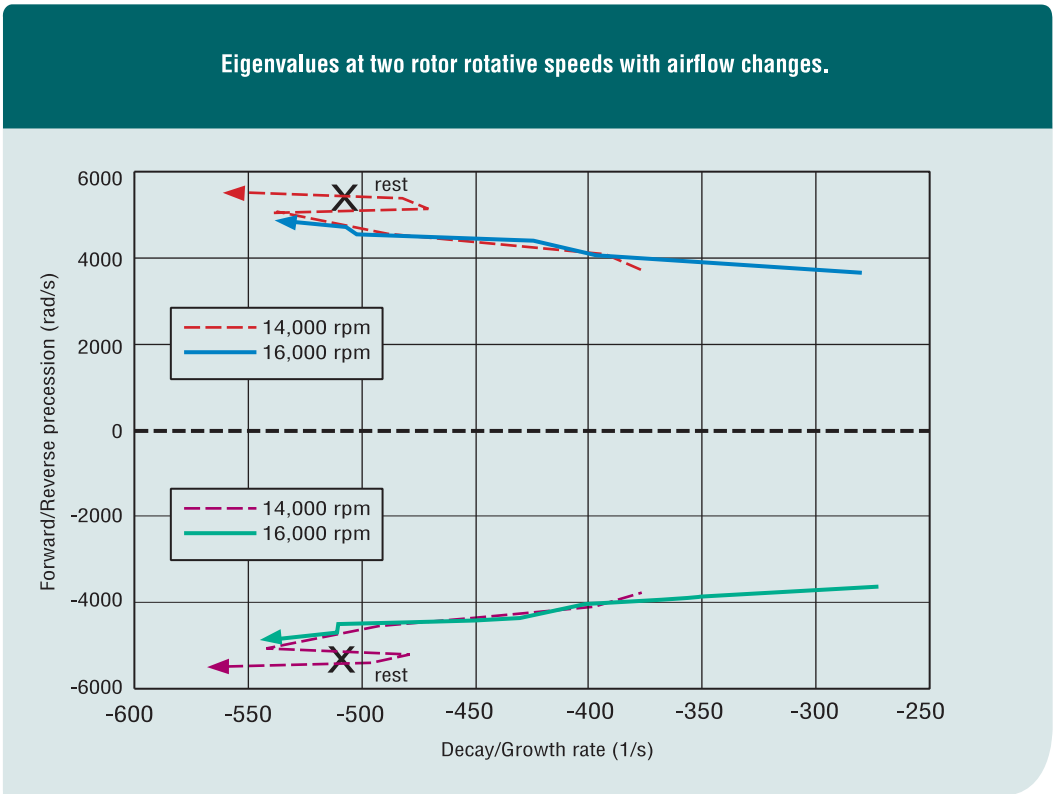

Figure 15.

References

1. Fowlie, D.W., Miles, D.D., (1975) "Vibration Problems With High Pressure Centrifugal Compressors," *ASME 75-Pet-28, Petroleum Mechanical Engrg. Conf.*, Tulsa, Oklahoma.
2. Smith, K.J., (1975) "An Operation History of Fractional Frequency Whirl," *Proceedings of 4th Turbomachinery Symposium*.
3. Wachel, J.C., (1975) "Nonsynchronous Instability of Centrifugal Compressors," *ASME 75-Pet-22*.
4. Ferrara, P., (1977) "Vibrations in Very High Pressure Centrifugal Compressors," *ASME 77-Det-15*.
5. Kaneki, T., Eino, T., (1979) "Centrifugal Compressor for Urea Synthesis Plant," *Hitachi Review,* Vol. 28, No. 6.
6. Ek, M.C., (1978) "Solution of the Subsynchronous Whirl Problem in the High Pressure Hydrogen Turbomachinery of the Space Shuttle Main Engine," *AIAA/SAE 14th Joint Propulsion Conference*, Las Vegas, Nevada.
7. Geary, C.H., Damratowsky, L. P., Seyer, C., (1976) "Design and Operation of the World's Highest Pressure Gas Injection Centrifugal Compressor," *No. 0TC 2485*, presented at the *Offshore Technology Conference*, Houston, Texas.
8. Sabella, D., Terrinoni, L., Timori, A., (1981) "Full Load Testing of Centrifugal Natural Gas Injection Compressors," *Inst. Mech. Ing. Conference Publications*.
9. Coletti, N.J., Crane, M.E., (1981) "Centrifugal Compression on the Arun High Pressure Injection Project," *Inst. Mech. Ing. Conference Publications*.
10. Bonciany, L., Ferrara, P.L., Timori, A., (1980) "Aero-Induced Vibrations in Centrifugal Compressors," *Workshop on Rotordynamic Instability* at Texas A&M University, Texas.
11. Bonciani, L., Terrinoni, L., Tesei, A., (1982) "Unsteady Flow Phenomena in Industrial Compressor Stage," *NASA Conference Publication 2250*.
12. Excerpts From Turbomachinery Technology Seminar, 11-14 March 1984, Coronado, California.
13. Wendt, P.G., (1985) "Forced Low Frequency Vibration Due to Aerodynamic Flow Instability (Rotating Stall)," *Solar Turbines, Inc., Engineering Report 2832*.
14. Fulton, J.W., (1986) "Subsynchronous Vibration of a Multistage Centrifugal Compressor Forced by Rotating Stall," *Turbomachinery Technology Seminar 1986,* Solar Turbines, Inc., San Diego, California, February.
15. Emmons, H.W., Pearson, C.E., Grant, H.P., (1955) "Compressor Surge and Stall Propagation," *Trans. ASME,* Vol. 79.
16. Lennemann, E., Howard, J.H.G., (1970) "Unsteady Flow Phenomena in Rotating Centrifugal Impeller Passages," *ASME 69-GT-35, ASME Journal of Engrg. for Power,* Vol. 108.
17. Frigne, P., Van den Braembusse, R., (1984) "Distinction Between Different Types of Impeller and Diffuser Rotating Stall in a Centrifugal Compressor With Vaneless Diffuser," *ASME Journal of Engrg. for Gas Turbines and Power,* Vol. 106, No. 2.
18. Van den Braembusse, R., (1987) "Rotating Stall in Centrifugal Compressors," *von Karman Institute for Fluid Dynamics*, Preprint, Belgium.
19. Haupt, U., Seidel, U., Abdel-Hamid, A.N., Rautenberg, M., "(1988) Unsteady Flow in a Centrifugal Compressor With Different Types of Vaned Diffusers," *ASME 88-GT-22*.
20. Jin, D., Haupt, U., Hasemann, H., Rautenberg, M., (1992) "Blade Excitation by Circumferentially Asymmetric Rotating Stall in Centrifugal Compressors," *ASME 92-GT-148*.
21. Chen, J., Huang, X., Hasemann, H., Seidel, U., Jin, D., Rautenberg, M., (1993) "The Interpretation of Internal Pressure Patterns of Rotating Stall in Centrifugal Compressor Impellers," *ASME 93-GT-192*.
22. Tsujimoto, Y., Acosta, A.J., (1987) "Theoretical Study of Impeller and/or Diffuser Attributed Rotating Stalls and Their Effects on Whirling Instability of a Centrifugal Impeller," *Work Group of Hydraulic Machinery Under Steady Oscillatory Conditions*, Lille, France.
23. Pampreen, R.C., (1993) "Compressor Surge and Stall," *Concepts ETI, Inc*., Norwich, Vermont.
24. Bently, D.E., Muszynska, A., (1988) "Role of Circumferential Flow in the Stability of Fluid-Handling Machine Rotors," *The 5th Workshop on Rotordynamic Instability Problems in High Performance Turbomachinery*, Texas A&M University, College Station, Texas, NASA CP 3026.
25. Muszynska, A., Bently, D.E., (1990) "Frequency Swept Rotating Input Perturbation Techniques and Identification of the Fluid Force Models in Rotor/Bearing/Seal Systems and Fluid-Handling Machines," *Journal of Sound and Vibration*, Vol. 143, No. 1.
26. Colding-Jorgensen, J., (1993) "Rotordynamic Effects of Impeller Flow in Centrifugal Compressors," *VDI Bevichte, No. 1082*.
27. Bently, D.E., Goldman, P., (1998) "Destabilizing Effect of Aerodynamic Forces in Centrifugal Compressors," *ISROMAC-7*, Honolulu, Hawaii.
28. Sorokes, J.M., Marshall D.F., (1998) "A Review of Aerodynamically Induced Forces Acting on Centrifugal Compressors, and Resulting Vibration Characteristics of Rotors," *Proceedings of the 27th Turbomachinery Symposium*, Texas A&M.
29. Bently, D.E., Goldman, P., (2000) "Vibrational Diagnostics of Rotating Stall in Centrifugal Compressors," *ORBIT*, Vol. 21 No. 1, Bently Nevada Corporation.